Broadband switching functionality based on defect mode coupling in W2 photonic crystal waveguide

Kaiyu Cui, Xue Feng, Yidong Huang, Qiang Zhao, Zhilei Huang et al.

Citation: Appl. Phys. Lett. **101**, 151110 (2012); doi: 10.1063/1.4758471
View online: http://dx.doi.org/10.1063/1.4758471
View Table of Contents: http://apl.aip.org/resource/1/APPLAB/v101/i15
Published by the American Institute of Physics.

Broadband switching functionality based on defect mode coupling in W2 photonic crystal waveguide

Kaiyu Cui, Xue Feng, Yidong Huang,[a] Qiang Zhao, Zhilei Huang, and Wei Zhang
Department of Electronic Engineering, State Key Laboratory of Integrated Optoelectronics, Tsinghua University, Beijing 100084, China

(Received 17 May 2012; accepted 25 September 2012; published online 9 October 2012)

Broadband switching functionality realized by an ultra-compact W2 photonic crystal waveguide (PCW) is demonstrated with an integrated titanium/aluminum microheater on its surface. Due to the enhanced coupling between the defect modes in W2 PCW, switching functionality with bandwidth up to 24 nm is achieved by the PCW with footprint of only 8 μm × 17.6 μm, while the extinction ratio is in excess of 15 dB over the entire bandwidth. Moreover, the switching speed is measured by alternating current modulation. Response time for this thermo-optic switch is 11.0 ± 3.0 μs for rise time and 40.3 ± 5.3 μs for fall time, respectively. © *2012 American Institute of Physics*. [http://dx.doi.org/10.1063/1.4758471]

Compact, low power consumption, and complementary metal–oxide–semiconductor (CMOS) compatible optical switches are essential elements for network-on-chip.[1,2] In addition, broadband switching functionality is also expected for wavelength division multiplexing (WDM) optical links in on-/off-chip communication.[3,4] For such applications, the preponderant candidate is silicon optical switch, which could be realized by thermo- or electro-optic effect. Among the reported silicon optical switches, microring resonator switch has been demonstrated with compact footprint and low power consumption, but it suffers from the sensitivity to thermal fluctuations or fabrication imperfections as well as very narrow operating bandwidth.[5] For broadband operation, Mach–Zehnder interferometers (MZIs) are commonly employed. However, the arm length of silicon based MZIs is usually as long as several millimeters to achieve π phase-shift.[4] Even though photonic crystal waveguides (PCWs) have been introduced into MZIs for shortening the length of phase shifter[6–8] with the help of the slow light enhancement of light-matter interactions,[9–12] the size for the PCW–MZIs reported up to now is still larger than 80 μm with operating bandwidth of 11 nm (Ref. 7) or 18 nm.[13] In our previous work,[14,15] we have proposed a different approach for optical switches, which relies on the defect mode coupling in photonic band gap (PBG). Based on such unique operating principle, the mode coupling strength in PBG can be flexibly controlled by proper designing of the PCW. Both low switching power consumption (9.2 mW) and high extinction ratio (17 dB) are experimentally achieved, however, the operating bandwidth is relative narrow (0.6 nm).

In this paper, we propose an upgraded solution to obtain broadband switches, which is based on the enhanced defect mode coupling in W2 PCW. The broadband operation of proposed ultra-compact switch is theoretically and experimentally demonstrated by the W2 PCW with integrated titanium (Ti)/aluminum (Al) microheater on top, and the footprint of the waveguide is only 8 μm × 17.6 μm. The bandwidth as high as 24 nm (from 1557 nm to 1581 nm) is achieved, meanwhile, the extinction ratio is larger than 15 dB over the entire bandwidth. Furthermore, the switching speed is measured by alternating current (AC) modulation. Response time for this thermo-optic switch is 11.0 ± 3.0 μs for rise time and 40.3 ± 5.3 μs for fall time, respectively.

The schematic of our proposed device is shown in Fig. 1(a). There are a PCW fabricated on silicon on insulator (SOI) substrate and an integrated Ti/Al microheater on top. The PCW is designed as a line-defect PBG-guiding waveguide with defect width of $W = (m + 1) \times (\sqrt{3}/2)a$, where a is the lattice period and m can be set for a certain width. Thus, the PCW with different defect widths can be denoted as Wm, such as the typical W1 or W3 PCW with defect

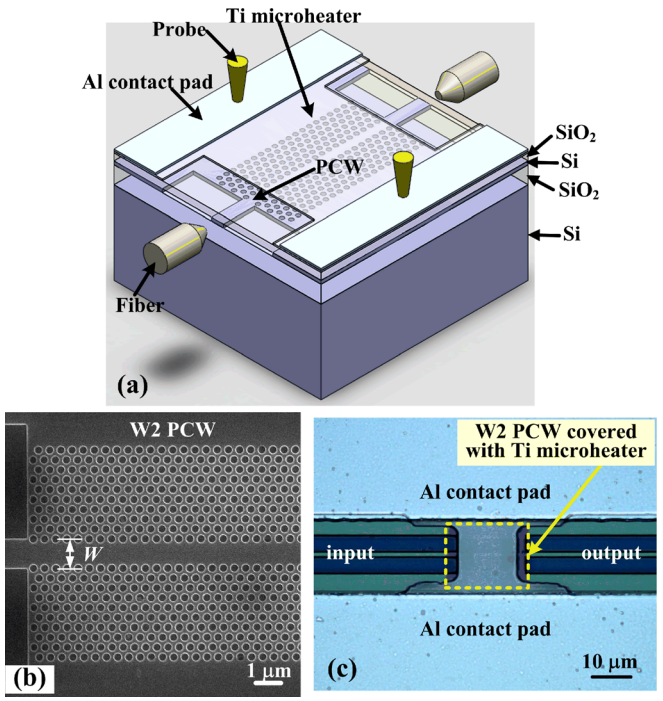

FIG. 1. (a) Schematic diagram of the proposed device; (b) the SEM image of the W2 PCW, where the lattice constant, a, and the hole radius, r, are 440 nm and 145 nm, respectively; (c) optical microscope picture of the fabricated W2 PCW with its titanium (Ti)/aluminum (Al) microheater.

[a]Electronic mail: yidonghuang@tsinghua.edu.cn.

width of one or three rows of missing holes while $m = 1$ or 3, respectively. In this paper, we design a W2 PCW with $m = 2$ to realize broadband switching functionality.

The scanning electron microscope (SEM) image for the W2 PCW fabricated on SOI wafer with a 230-nm-thick silicon top layer is given in Fig. 1(b), where the footprint is $8\,\mu m \times 17.6\,\mu m$ and the lattice constant (a) and the hole radius (r) is 440 nm and 145 nm, respectively. On top of the W2 PCW, a 600-nm-thick SiO_2 cladding layer is deposited to form both optical and electrical isolations, as well as to form a vertical symmetric waveguide structure for improving the end-fire coupling efficiency. Then, an integrated microheater is fabricated above the SiO_2 layer, and the optical micrograph for the finally fabricated sample is presented in Fig. 1(c). The microheater is designed as a Ti rectangular slab with size of $14\,\mu m \times 15\,\mu m$ and thickness of 100 nm. In addition, two Al electrical contact pads are deposited on the top and both sides of the Ti microheater to reduce the contact resistance, as depicted in Fig. 1(c). The resistance of the microheater (including contact pads) is measured as 60 Ω.

In order to demonstrate the operating principle for the broadband operation, the band structure and transmission spectra of the W2 PCW are provided in Fig. 2. The band structure and transmission spectra of the transverse electric (TE) mode are calculated by two dimensional (2D) plane wave expansion (PWE) method and 2D finite-difference time-domain (FDTD) method. Here, the effective refractive index of W2 PCW is set as $n_{eff} = 2.7$, while the structure parameters are consistent with the fabricated sample. Due to the unique guiding mechanism of PBG effect, PCW offers the possibility to guide light in the line defect waveguide and Bragg couplings between the defect modes. It can be seen from Fig. 2(a) that there is mode coupling between the fundamental mode (#0) and the higher order mode (#2), so that in the frequency range of the fundamental mode, mini-gaps so-called mini-stopbands (MSB)[16] appear. For more clarity, an enlarged figure for the mode coupling region is highlighted in the inset of Fig. 2(a) as rectangular box. With the help of the slow light effect, mode coupling in the W2 PCW can be enhanced to obtain larger MSB bandwidth. The calculated MSB bandwidth ΔU for the proposed W2 PCW is up to 6.1×10^{-3}. It should be mentioned that ΔU for W3 PCW is only 2.5×10^{-3}.[16] So owing to the enhanced mode coupling between modes #0 and #2 with a large ΔU, a transmission-dip could be obtained over rather wide wavelength range of 35 nm with a single W2 PCW, while the length is only $40\,a$ ($17.6\,\mu m$), as shown in Fig. 2(b). Besides the bandwidth, the depth of a transmission-dip is another key factor that should be considered since it is directly related to the switching extinction ratio. To achieve a deep transmission-dip, the W2 PCW is carefully designed by optimizing the structure parameters including the radius, r, and the lattice period, a. As shown in Fig. 2(b), the extinction ratio could be as high as 45 dB under the optimized $a = 440$ nm and $r = 145$ nm. The transmission dip under different variations of the refractive index (Δn) is also numerically simulated and shown in Fig. 2(b). It can be seen that the transmission-dip shows a red-shift with an increased refractive index variation Δn, which corresponds to a temperature coefficient of $\Delta\lambda/\Delta T = 0.07\,nm \cdot K^{-1}$ with a thermo-optic coefficient of $\Delta n/\Delta T = 1.86 \times 10^{-4} \cdot K^{-1}$ for silicon.[17]

To achieve both high heating transfer efficiency and high thermal tuning efficiency, the steady-state thermal analysis is also performed to obtain the optimized design of the microheater. Three dimensional (3D) finite element method (FEM) is employed to model the temperature distribution and power consumption. The calculated region is fixed as $50\,\mu m \times 50\,\mu m \times 14\,\mu m$ to ensure that a room-temperature ($T = 293.15$ K) boundary condition is valid at the bottom of the device. The convective cooling boundary is exploited for the other surfaces with a heat transfer coefficient of $5\,W/(m^2 \cdot K)$. The simulated temperature distribution with a heating power of $P = 59$ mW is given in Fig. 3(a). The heating temperature can be varied by proper setting of the heating power, and the results are shown in Fig. 3(b). The blue and red lines are the calculated temperature variations (ΔT) versus the applied power at the centers of the microheater and the PCW, respectively. As the temperature increases proportionally to the applied heating power, we define a parameter η named heating transfer efficiency that is the ratio of the ΔT for the PCW to that of the microheater: $\eta = \Delta T_{PCW}/\Delta T_{Microheater}$. Deduced from the results in Fig. 3(b), the heating efficiency for the proposed device is as high as 72%. Taking account of the temperature coefficient of $\Delta\lambda/\Delta T = 0.07\,nm \cdot K^{-1}$ for the W2 PCW, the simulated thermal tuning efficiency[5] for our proposed device can be

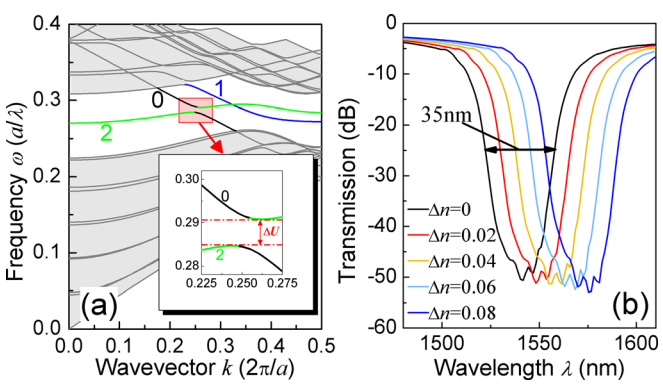

FIG. 2. (a) TE mode band structure and (b) transmission spectra under different refractive index variations of the W2 PCW with structure parameters: $a = 440$ nm and $r = 145$ nm.

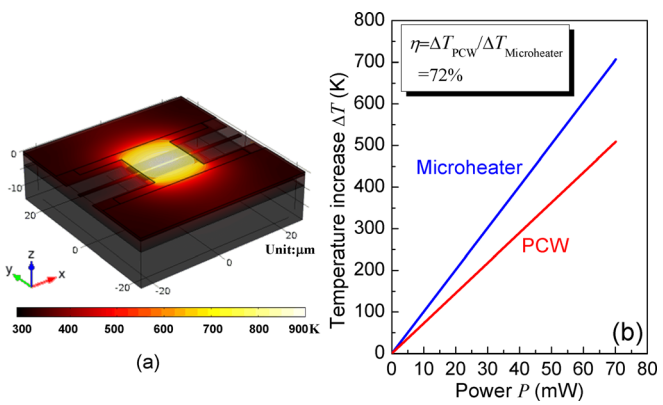

FIG. 3. (a) Three dimensional temperature distribution with a heating power of $P = 59$ mW; (b) temperature increase under different applied heating powers.

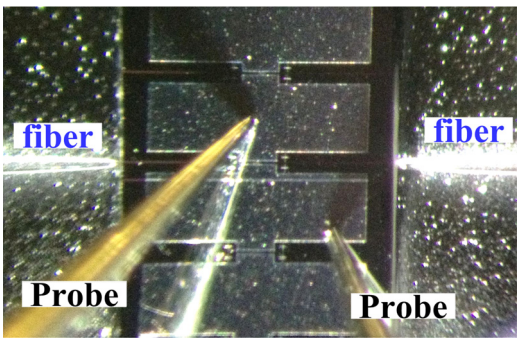

FIG. 4. Microscope picture of the measured W2 PCW with input- and ouput-fibers. Here, the two electrical probes are used to apply a potential on two Al contact pads of the microheater.

calculated and the value is 509 pm/mW, which is very preferable for realizing low power devices.

The switching performance is measured by applying a potential through two electrical probes on Al contact pads of the microheater as shown in Fig. 4. The measured transmission spectra under different heating power are presented in Fig. 5(a). The insertion loss for our proposed PCW is 1.5 ± 0.5 dB, which is obtained by comparing with a straight waveguide. It can be seen that the transmission-dip is deeper than 20 dB without applying power. While the applied heating power varying within the range of 0-154.1 mW, the transmission-dip could be shifted to longer wavelengths with $\Delta\lambda = 31$ nm. Therefore, the thermal tuning efficiency could be obtained as high as 201 pm/mW which is much larger than the reported data for the microring resonator based device (90 pm/mW).[5] The spectrum red-shift of 31 nm for the W2 PCW corresponds to a temperature increase of 443 K which can be calculated from the temperature coefficient of $\Delta\lambda/\Delta T = 0.07\ \text{nm} \cdot \text{K}^{-1}$. Thus, the theoretical heating power to obtain such a temperature variation is 61 mW with the results in Fig. 3(b). The difference of the power consumption (or thermal tuning efficiency) between the experimental and the theoretical values is mainly caused by the power dissipating of the practical device due to the surface-to-ambient heat radiation and convective cooling process.

Based on shifting the transmission-dip, broadband switching functionality is observed in W2 PCW. The extinction ratio under different heating power is shown in Fig. 5(b). It can be seen from Fig. 5 that within the wavelength

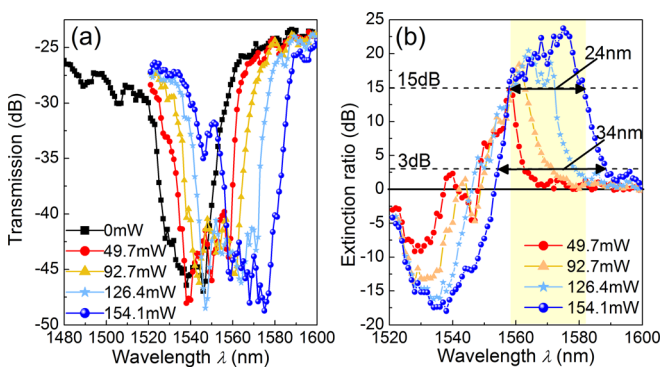

FIG. 5. (a) Measured transmission spectra under different applied heating powers, here the time frame needed to take data is 24 s; (b) extinction ratio of the switching on- and off-state.

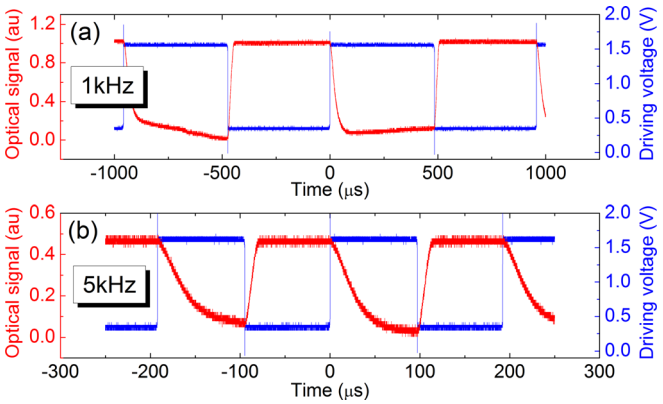

FIG. 6. Measured optical response of the output port of the optical switch at a fixed optical wavelength of 1563 nm, as it is driven by (a) 1 kHz and (b) 5 kHz rectangular wave signals.

range of 1557–1581 nm for our fabricated sample, the switch is at on-state without heating power and turned to off-state with applied power of 154.1 mW, while the extinction ratio is higher than 15 dB. This experimental result indicates that switching functionality with bandwidth up to 24 nm is achieved by the W2 PCW. Considering the footprint of only $8\ \mu\text{m} \times 17.6\ \mu\text{m}$, the proposed W2 PCW provides a practical solution for broadband and ultra-compact switch.

Moreover, the switching speed is measured by AC modulation. Figure 6 shows the measured optical response at the output port of the optical switch driven by 1 kHz (top) and 5 kHz (bottom) rectangular wave signals with a fixed optical wavelength of 1563 nm. From the multiple-sampling measurements, the rise time and fall time for this thermo-optic switch are $11.0 \pm 3.0\ \mu\text{s}$ and $40.3 \pm 5.3\ \mu\text{s}$, respectively. Based on these values, the response bandwidth is about 15 kHz. Obviously, the proposed device is not suitable for serving as a modulator for network-on-chip applications, whereas it is promising as a broadband optical switch. The power consumption can be estimated by assuming the channel spacing and data rate as 0.4 nm (50 GHz Grid) and 10 Gb/s according to the International Telecommunication Union (ITU) standard. For our demonstrated device, the heating power is 154.1 mW within the wavelength span of 24 nm, so the power consumption per bit is only 0.26 pJ/bit. This value is comparable with the power consumption of 0.54 pJ/ bit reported in Ref. 18.

In conclusion, we propose and demonstrate an ultra-compact W2 PCW to realize the broadband switching functionality based on the defect modes coupling. The operation bandwidth could be as broad as 24 nm (from 1557 nm to 1581 nm) with extinction ratio more than 15 dB, while the footprint of the fabricated W2 PCW is only $8\ \mu\text{m} \times 17.6\ \mu\text{m}$. What is more, the switching speed is measured by AC modulation. Response time for this thermo-optic switch is $11.0 \pm 3.0\ \mu\text{s}$ for rise time and $40.3 \pm 5.3\ \mu\text{s}$ for fall time, respectively. This experimental result shows the potential of the proposed W2 PCW in broadband switching applications for network-on-chip.

This work was supported by the National Basic Research Program of China (Nos. 2011CBA00608, 2011CBA00303, and 2010CB327405), the National Natural

Science Foundation of China (Grant Nos. 61036011 and 61036010), and China Postdoctoral Science Foundation. The authors would like to thank Dr. Fang Liu for his valuable discussions.

[1]H. Lira, S. Manipatruni, and M. Lipson, Opt. Express **17**, 22271 (2009).
[2]D. Miller, IEEE Proc. **97**, 1166 (2009).
[3]Y. Vlasov, W. Green, and F. Xia, Nat. Photonics **2**, 242 (2008).
[4]P. Dong, S. R. Liao, H. Liang, R. Shafiiha, D. Z. Feng, G. L. Li, X. Z. Zheng, A. V. Krishnamoorthy, and M. Asghari, in 2011 Optical Fiber Communication Conference (OFC), Los Angeles, California, 6 March 2011, Silicon Photonics II (OWZ), paper OWZ4.
[5]X. Z. Zheng, I. Shubin, G. L. Li, T. Pinguet, A. Mekis, J. Yao, H. Thacker, Y. Luo, J. Costa, K. Raj, J. E. Cunningham, and A. V. Krishnamoorthy, Opt. Express **18**, 5151 (2010).
[6]L. L. Gu, W. Jiang, X. N. Chen, and R. T. Chen, IEEE Photonics Technol. Lett. **19**, 342 (2007).
[7]L. O'Faolain, D. M. Beggs, T. P. White, T. Kampfrath, K. Kuipers, and T. F. Krauss, IEEE Photonics J. **2**, 404 (2010).
[8]H. C. Nguyen, Y. Sakai, M. Shinkawa, N. Ishikura, and T. Baba, Opt. Express **19**, 13000 (2011).
[9]Y. Q. Jiang, W. Jiang, L. L. Gu, X. N. Chen, and R. T. Chen, Appl. Phys. Lett. **87**, 221105 (2005).
[10]Y. A. Vlasov, M. O'Boyle, H. F. Hamann, and S. J. McNab, Nature **438**, 65 (2005).
[11]T. Baba, Nat. Photonics **2**, 465 (2008).
[12]K. Y. Cui, Y. D. Huang, W. Zhang, and J. D. Peng, J. Lightwave Technol. **26**, 1492 (2008).
[13]A. Hosseini, X. C. Xu, H. Subbaraman, C. Y. Lin, S. Rahimi, and R. T. Chen, Opt. Express **20**, 12318 (2012).
[14]K. Y. Cui, Y. D. Huang, G. Y. Zhang, Y. Z. Li, X. Tang, X. Y. Mao, Q. Zhao, W. Zhang, and J. D. Peng, Appl. Phys. Lett. **95**, 191901 (2009).
[15]K. Y. Cui, Q. Zhao, X. Feng, Y. D. Huang, Y. Z. Li, D. Wang, and W. Zhang, Appl. Phys. Lett. **100**, 201102 (2012).
[16]S. Olivier, H. Benisty, C. Weisbuch, C. Smith, T. Krauss, and R. Houdre, Opt. Express **11**, 1490 (2003).
[17]G. Coppola, L. Sirleto, I. Rendina, and M. Iodice, Opt. Eng. **50**, 071112 (2011).
[18]X. N. Chen, Y. S. Chen, Y. Zhao, W. Jiang, and R. T. Chen, Opt. Lett. **34**, 602 (2009).